AIP | Review of Scientific Instruments

A new version of the LUPIN detector: Improvements and latest experimental verification

M. Caresana, C. Cassell, M. Ferrarini, E. Hohmann, G. P. Manessi, S. Mayer, M. Silari, and V. Varoli

Citation: Review of Scientific Instruments **85**, 065102 (2014); doi: 10.1063/1.4879936
View online: http://dx.doi.org/10.1063/1.4879936
View Table of Contents: http://scitation.aip.org/content/aip/journal/rsi/85/6?ver=pdfcov
Published by the AIP Publishing

A new version of the LUPIN detector: Improvements and latest experimental verification

M. Caresana,[1] C. Cassell,[1,2] M. Ferrarini,[3] E. Hohmann,[4] G. P. Manessi,[5,6,a)] S. Mayer,[4] M. Silari,[5] and V. Varoli[1]
[1]*Department of Energy, Polytechnic of Milan, Via Ponzio 34/3, 20133 Milan, Italy*
[2]*Centre for Medical Physics, University of Wollongong, NSW 2522, Australia*
[3]*CNAO, Via Privata Campeggi, 27100 Pavia, Italy*
[4]*Paul Scherrer Institut, 5232 Villigen, Switzerland*
[5]*CERN, 1211 Geneva 23, Switzerland*
[6]*Department of Physics, University of Liverpool, L69 7ZE Liverpool, United Kingdom*

(Received 7 March 2014; accepted 14 May 2014; published online 3 June 2014)

LUPIN-II is an upgraded version of LUPIN, a novel rem counter first developed in 2010 specifically conceived to work in pulsed neutron fields (PNFs). The new version introduces some modifications that improve the performance of the detector, in particular extending its upper detection limit in PNFs. This paper discusses the characteristics and the performance of the instrument. Measurements have been carried out in radiation fields characterized by very different conditions: the detector has first been exposed in PNFs with intensity up to 5 μSv per burst, where it could keep the H*(10) underestimation below 20% up to 500 nSv per burst. It has then been tested in operational conditions around particle accelerators, where it has shown performances similar to that of ionization chambers. Its proper functioning has also been verified in high energy mixed fields, where the experimental results matched the Monte Carlo predictions. Its neutron/photon discrimination capability has been tested in a steady-state photon field where, via an innovative technique based on a threshold set on the derivative of the current signal, it was capable of rejecting a photon H*(10) rate of about 25 mSv/h, and in a mixed neutron/photon field, where a time-based discrimination method was employed.
 [http://dx.doi.org/10.1063/1.4879936]

I. INTRODUCTION

A radiation detector can operate in three different modes: current, mean square voltage (MSV), and pulse mode. Current mode averages out the fluctuations in the intervals between individual interactions and is usually employed with high interaction rates. MSV mode is useful when making measurements in mixed radiation environments when the charge produced by one type of radiation is much different than that from the second type. Pulse mode is the most commonly applied, especially for applications that are better served by preserving information on the amplitude and timing of individual events. This is the case for most neutron detectors where the output usually consists of a sequence of individual pulses, each representing the results of a single interaction. One of the advantages of pulse mode operation is that the sensitivity is greater than when using current or MSV mode, because each interaction can be detected as a distinct pulse. This is a desirable property for radiation protection measurements because of the low detection limits required. The downside is represented by the dead time losses induced by the counting system, which can be correctly compensated only in the case of steady-state sources of constant intensity, but not in the case of pulsed sources.[1]

Severe under response has been observed in commercial rem counters with underestimations of the ambient dose equivalent, H*(10), up to three orders of magnitude[2] when they are employed in pulsed neutron fields (PNFs). The detection limit in a PNF for a rem counter can be quantified by assuming typical values of dead time τ, sensitivity k, and thermalization and diffusion time TDT of the neutrons in the moderator (usually a few hundred microseconds[3]): $\tau = 5$ μs, $k = 1$ nSv^{-1}, and TDT $= 500$ μs. If the duration of the burst, characterized by a certain H*(10), is shorter than TDT, the interaction rate in the burst is:

$$\frac{H^*(10) \cdot k}{TDT}. \tag{1}$$

To limit the underestimation the maximum interaction rate must be lower than $(10 \cdot \tau)^{-1}$, i.e., 2×10^4 s^{-1} with the above parameters. The maximum H*(10) per burst that the detector can withstand is then about 10 nSv, which is a stringent limit. The lack of neutron survey meters capable to efficiently operate in PNFs represents an important issue in radiation protection.

A promising approach that overcomes the limitations described above has been proposed by Caresana *et al.*,[4,5] with the development of a new instrument, LUPIN, with a front-end electronics based on a current to voltage logarithmic amplifier (LogAmp) that permits the reconstruction of the time profile of the neutron interactions. LUPIN was originally conceived as beam loss monitor (BLM) for hadrontherapy accelerators,[4] specifically for the CNAO clinical proton synchrotron,[6] and subsequently developed as a rem counter, given the potentialities it showed for radiation protection applications. The signal is digitally handled and the charge

a)Author to whom correspondence should be addressed. Electronic mail: giacomo.manessi@cern.ch

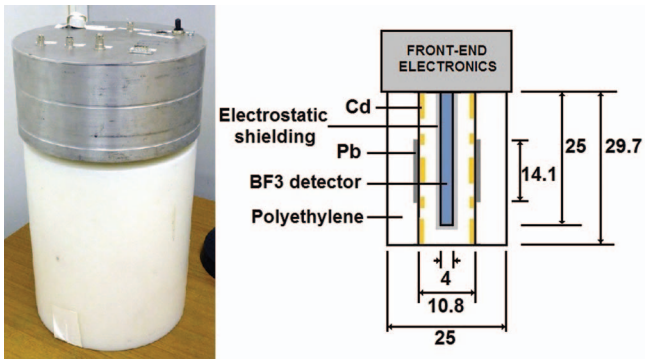

FIG. 1. Photograph and sketch of the LUPIN-II moderator (dimensions in centimeters).

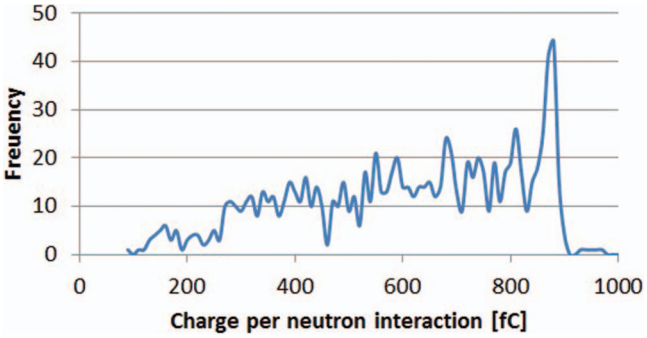

FIG. 2. Charge per neutron distribution.

produced in the gas is calculated by integrating the current over a settable time base. This allows measuring the generated charge even if the neutron interactions pile up. The total charge divided by the average charge expected by a single interaction represents the number of interactions occurring during the integration time. Its sensitivity is typical of a rem counter and its response is linear up to 16 nSv per burst, with an underestimation of H*(10) of 40% at 92 nSv per burst. To further improve the performance in PNFs, a new version of the detector, LUPIN-II, has been developed. This paper discusses the modifications introduced in LUPIN-II, describes its calibration and presents the results of several measurement campaigns. For some of these campaigns, the measurements were performed in the framework of large intercomparisons, which involved a considerable number of detectors and whose detailed descriptions are given elsewhere. The results presented in this paper focus on the performance of LUPIN-II and are meant to give a complete overview of the different conditions in which the detector has been tested.

II. MATERIALS AND METHODS

LUPIN-II is a rem counter type instrument consisting of a cylindrical BF_3 proportional counter (Centronics 15EB/20/25SS) with gas pressure of 200 mmHg (26664 Pa) placed at the center of a cylindrical moderator (Fig. 1). It shares the front end electronics of LUPIN, whose working principle is thoroughly described in Ref. 5. The operating voltage is 1180 V. The output signal is acquired by an analog-to-digital converter (ADC) with a conversion rate of 10 MSamples/s. The ADC output is processed with a LabVIEW program. The replacement of the spherical ^{3}He with the BF_3, which was originally chosen as the active gas for the first version of the prototype,[4] offers some advantages: higher Q-value of the $^{10}B(n,\alpha)^7Li$ reaction when compared to the $^3He(n,p)^3H$, which results in a better photon rejection; larger active volume (25 mm diameter and 150 mm length for the BF_3, 31 mm diameter for the ^{3}He), which reflects in a mitigation of the space charge effect. This effect is generated when a large number of neutron interactions occur in the gas in a very short time: the space charge causes a reduction in the electric field around the anode and consequently a decrease in the multiplication factor. Its importance is reduced if larger active volumes are employed.[7] The downsides are represented by the loss of an isotropic response (due to the cylindrical geometry of the BF_3) and a reduced sensitivity. The moderator consists of a polyethylene cylinder of 25 cm diameter with lead and cadmium inserts. An electrostatic shielding, constituted by an aluminum cylinder of 1.5 mm thickness, contains the detector and two polyethylene inserts, which are used to fill the void around the detector.

III. RESULTS AND DISCUSSION

A. Calibration

The characterization of the detector requires the knowledge of the mean collected charge (MCC), expressed in fC, i.e., the average amount of charge generated in the detector by a neutron interaction, and the conversion coefficient from neutron interactions to H*(10), expressed in nSv^{-1}. The calibration in charge was performed at the Polytechnic of Milan with an Am-Be source. The source-detector distance was tuned in order to obtain about 10 s^{-1} interactions. Several integration times where used, ranging from 500 μs to 4 ms. Figure 2 shows the normalized distribution, where the full energy deposition peak and the wall effect continuum are visible. The MCC is defined as the weighted average of the charge distribution. It depends on the detector, the operating voltage and the integration time (Table I): it reaches a plateau for integration times longer than 1 ms. For lower values the charge collection is incomplete due to the ballistic deficit,[8] i.e., the difference in the amplitude of the pulse if compared to that attainable with an acquisition system characterized by an infinite time constant.

The calibration in H*(10) was performed in the CERN calibration laboratory with a Pu-Be source. The integration time was set at 2 ms. The calibration factor is 2.13 $\pm$ 0.17 nSv^{-1}, where the uncertainty derives from the

TABLE I. Values of MCC calculated for several integration times.

Integration time (ms)	MCC (fC)
0.5	547
1	616
2	611
3	616
4	617

calibration of the source (7%) and the counting statistics. In order to test the geometrical dependence of the response of LUPIN-II, the calibration was performed at different orientations along the three axes (turned by steps of 30° in each orientation). The results show that the response is not isotropic, but the differences in the calibration factor are included in a ±20% variation.

B. Measurements in pulsed neutron fields

At the Helmholtz-Zentrum Berlin (HZB), the response linearity was tested by irradiating the detector in a reference position with neutrons delivered in bursts of different intensity. At the High Irradiation to Materials (HiRadMat) facility at CERN, LUPIN-II was exposed to a stray field whose intensity was steadily increased in order to check the response linearity in conditions characterized by a significant scattered neutron component. It was also tested in operational conditions at the CERN Proton Synchrotron (PS).

1. Measurements at HZB

A 68 MeV proton beam accelerated by a cyclotron was delivered on a tungsten target and the detector was placed in a reference position at 50 cm distance. The beam current was varied between 0.5 pA and 3 nA and the burst length between 1 μs and 40 μs. Full details of the experiment are given in Ref. 9. Figure 3 shows the results obtained with LUPIN-II, LUPIN, and (for comparison) a Thermo BIOREM. The attention was focused on the loss of the response linearity. BIOREM and LUPIN deviate from linearity at 20 nSv/burst, with an underestimation of 45% for LUPIN and 60% for the BIOREM when the expected H*(10) is 154 nSv/burst. The response of LUPIN-II is linear up to 150 nSv/burst, with a 20% underestimation at 470 nSv/burst. It is worth noting that this corresponds to 10^3 interactions in a TDT of 500 μs, i.e., an interaction rate of about 2×10^6 s^{-1}.

2. Measurements at CERN HiRadMat

A 440 GeV/c proton beam was extracted from the Super Proton Synchrotron (SPS) and impinged on a beam dump. The beam intensity varied between 5×10^9 and 7.5

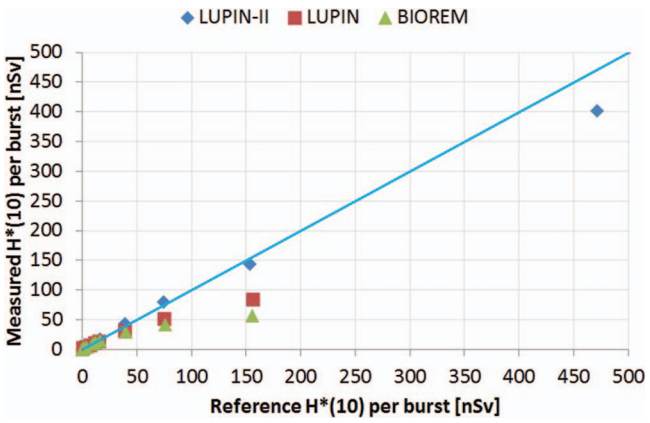

FIG. 3. LUPIN, LUPIN-II, and BIOREM response (measured vs expected H*(10) per burst) at HZB, compared with the ideal response (straight line).

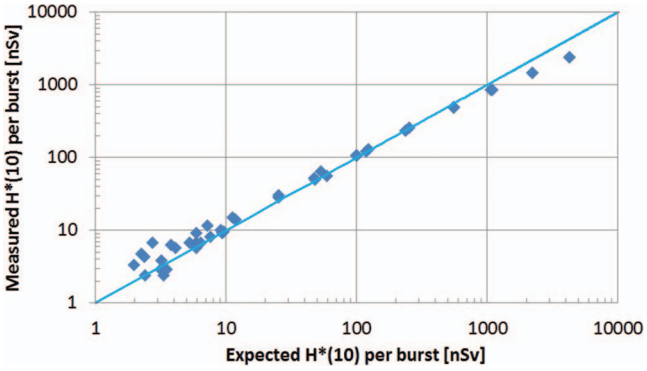

FIG. 4. LUPIN-II response (measured vs expected H*(10) per burst) at HiRadMat, compared with the ideal response (straight line).

$\times 10^{12}$ protons per SPS pulse and the pulse length between 50 ns and 28.8 μs. The detectors were installed at the end of a bent tunnel, 40 m far from the dump. The linearity of the response of LUPIN-II was compared with four detectors (two ionization chambers, filled with pressurized Argon and Hydrogen, and two rem counters, Thermo Wendi-II and BIOREM). Unlike in the measurements performed at HZB, the scattered component of the stray field was of great importance. A full description of the intercomparison is given in Ref. 10. The results obtained with LUPIN-II are shown in Fig. 4: the H*(10) underestimation is always limited within 20% up to 500 nSv/burst and reaches a maximum of 50% when the expected H*(10) is 5 μSv/burst. One would expect a lower underestimation of the detector in this experiment if compared to the HZB campaign, due to the fact that an important fraction of the stray field is scattered and delayed, resulting in a longer burst duration. However, the response linearity is lost at 500 nSv/burst (20% underestimation), similar to what was obtained at HZB. This can be explained considering that the influence of the space charge effect continues until the positive ions reach the cathode, i.e., for several hundred microseconds after the end of the burst, thus affecting also the delayed component of the neutron burst.

3. Measurements around CERN PS accelerator

Measurements were performed with LUPIN-II along with five detectors (Argon and Hydrogen filled ionization chambers and three rem counters: Wendi-II, BIOREM and the CERN LINUS[11–14]) at the entrance of a tunnel that gives access to the beam extraction section of the PS, where PNFs are generated by extraction losses. The intercomparison is thoroughly described in Ref. 15. The detectors were installed at a distance of 40 m from the loss point and their positions interchanged. The signal is spread out due to the multiple scattering events that the neutrons undergo on the tunnel walls. The results, normalized to the H*(10) integrated by a monitoring station installed at the tunnel entrance, are shown in Fig. 5. According to their responses, the detectors can be divided in three groups: (1) LUPIN-II and the two ionization chambers; (2) BIOREM; and (3) LINUS and Wendi-II. The first group shows results coherent with those obtained from FLUKA[16,17] Monte Carlo simulations, while the underestimation of the other two is more important as the dead time of

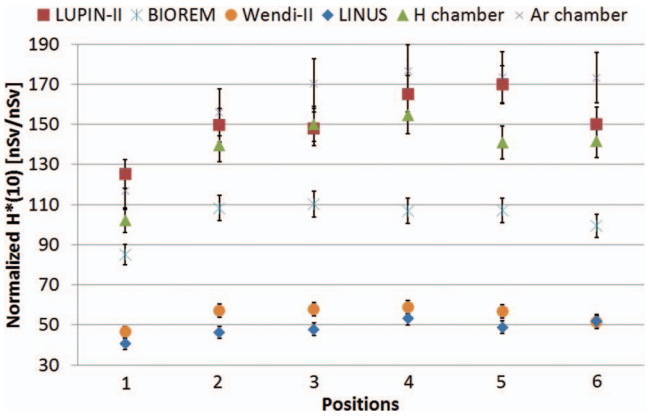

FIG. 5. Results of the instrument intercomparison at the CERN PS.

the instruments is higher (30% for the second group, which has a dead time of 1 μs; 60% for the third group, with 2 μs dead time). The results of LUPIN-II can be compared with the ionization chambers, which work in current mode and are not affected by dead time losses.

C. Measurements in high energy mixed fields

Measurements were carried out at the CERN-EU high-energy reference field (CERF) facility[18] to test the performance of LUPIN-II in high energy mixed fields. Although the detector is specifically conceived for PNFs, a test in operational non-pulsed conditions is necessary. The stray radiation field is generated by a 120 GeV/c hadron (protons/pions) beam impinging on a copper target. The secondary particles produced in the target traverse a concrete shield generating an almost uniform radiation field at 90° with respect to the incoming beam direction. The beam is delivered by the SPS with typical spill duration of about 10 s over an SPS cycle of about 45 s. The measurements were performed in several reference locations (see the supplementary material[19]). The integration time of LUPIN-II was set to 10 s. The results, obtained by normalizing the H*(10) to the integrated beam fluence were compared with FLUKA simulations. There is a good agreement between experimental and Monte Carlo results, though for some locations LUPIN-II seems to underestimate the H*(10) by 10%-20%. This slight difference has been noticed in similar experiments carried out in the past with other rem counters[20] and is probably due to the increased sensitivity of a rem counter when the stray field is partially directional and reaches the detector from the bottom, as it is the case for CERF. In this condition one should apply a correction to the calibration factor. If the standard calibration factor is used, as in these measurements, one obtains a slight underestimation of the neutron H*(10).

D. Neutron/photon discrimination

The neutron/photon discrimination properties of LUPIN-II were tested via measurements performed at the ACCREDIA (Italian National Centre for Accreditation) secondary standard calibration laboratory at the Polytechnic of Milan. The detector was exposed to an Am-Be source accompanied by a steady-state photon field produced by a ^{137}Cs source. Tests were also carried out at the Paul Scherrer Institute (PSI), Villigen, Switzerland, in a mixed neutron/photon pulsed field.

1. Measurements at the Polytechnic of Milan

LUPIN-II was simultaneously exposed to an Am-Be and a ^{137}Cs source. The photon H*(10) rate could be switched from 0 to about 25 mSv/h by opening a shutter, whereas the neutron interaction rate was kept constant to about 10 s^{-1}. The integration time was set to 10 ms. The signals obtained with the detector exposed to the Am-Be and ^{137}Cs sources separately and contemporaneously are shown in Fig. 6. The photon field increased the current baseline (which, in absence of external signal, is set to 160 pA to avoid the LogAmp inverse saturation) to a value fluctuating around 400 pA. The charge integration of the entire signal, without corrections, would lead to an overestimation of the neutron H*(10) by a factor of 10. On the other hand, an effective subtraction of the additional signal generated by the photon field is not possible, due to the substantial fluctuations in the current baseline.

Thus, in order to effectively distinguish the neutron/photon signal, a novel discrimination technique was employed. The technique (from now on called the "derivative technique") digitally reverts LUPIN-II into a detector operating in pulse mode, with the difference that the threshold is set on the derivative of the current signal, defined as

$$\frac{d(I_n)}{dt} = \frac{1}{2\delta t}(I_{n+1} - I_{n-1}), \tag{2}$$

where I_{n-1}, I_n, and I_{n+1} are the current values and δt is the time step (100 ns). The neutron signal is detected via a peak detection analysis, which requires a user settable number of samples to exceed the threshold before the signal is recognized as a neutron interaction. Figure 7 shows the comparative rising edge of several photon and neutron signals and the threshold level set for the derivative technique during the acquisitions, i.e., 0.5 mA/s.

In a steady photon field, the sudden increase in the signal caused by a neutron interaction allows the derivative technique to effectively discriminate a neutron interaction from the photon background. The time width of the derivative signal is around 1 μs, i.e., the rising edge of the primitive signal, which roughly corresponds to the detector dead time. The reliability of the derivative technique was tested by comparing the acquired neutron interaction rate in two conditions: (1) acquisition in streaming, by integrating the charge without having set a threshold; (2) by setting a threshold at 0.5 mA/s (the straight line in Fig. 7) on the derivative of the signal. The results are given in Table II by employing the derivative technique, the effect of the photon field on the acquired neutron interaction rate is negligible.

The electrons produced in the photoelectric reaction on the detector walls by the ^{137}Cs photons are not stopped in the gas and deposit only a fraction of their energy. In case of higher energy photons, the average electron energy would increase but this would result in a reduction of the mass

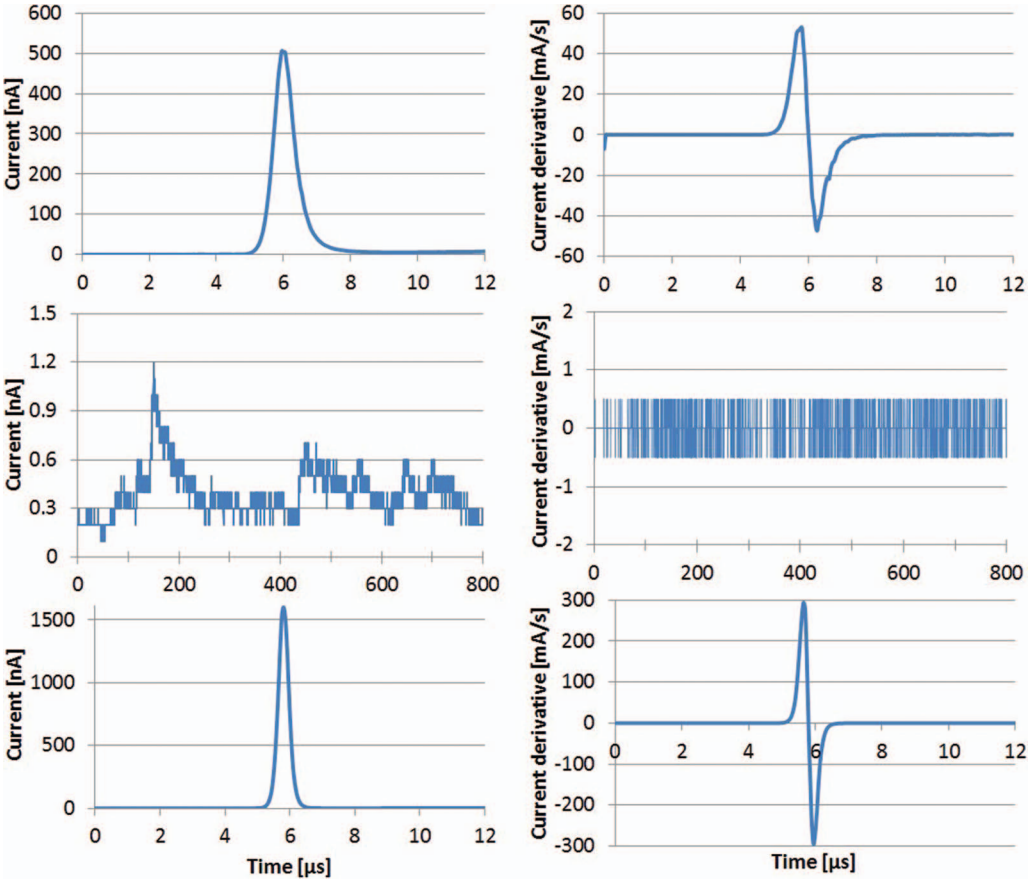

FIG. 6. Signals in current (left) and current derivative (right) acquired in a neutron (top), photon (center), and mixed field (bottom) at the Polytechnic of Milan.

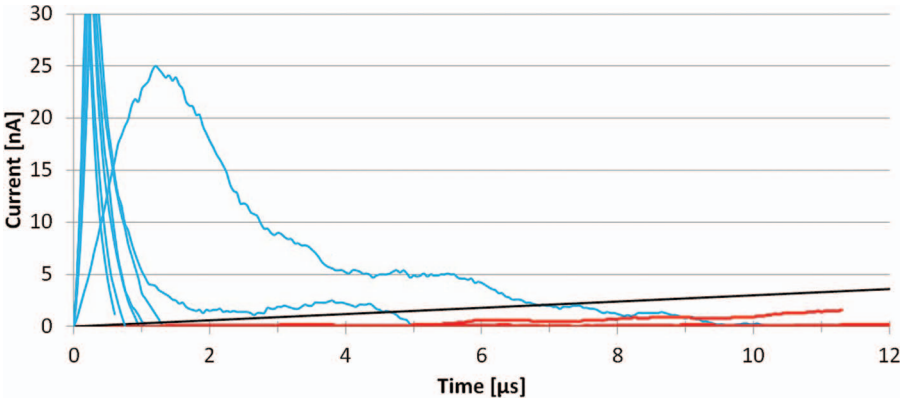

FIG. 7. Leading edges of neutron (blue curves) and photon signals (red dashed curves), together with the discrimination threshold set for the derivative technique (black straight line).

TABLE II. Comparison of the neutron interaction rate acquired in streaming and with the derivative technique.

Sources	Measurement	Streaming (s^{-1})	Derivative (s^{-1})
Am-Be	1	19.4 ± 4.4	19.6 ± 4.4
	2	20.5 ± 4.5	20.8 ± 4.6
Am-Be ^{137}Cs	3	495 ± 22	21.5 ± 4.6
	4	496 ± 22	20.9 ± 4.6

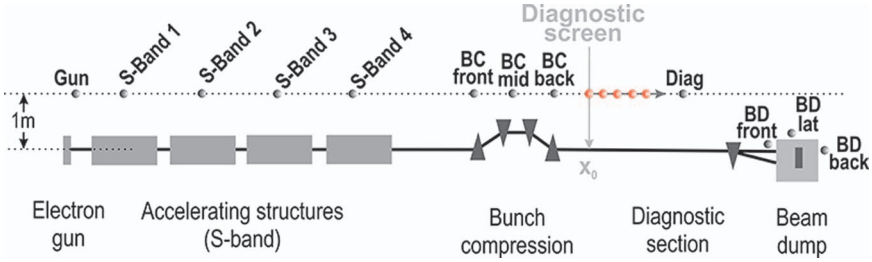

FIG. 8. Sketch of SwissFEL Injector Test facility: the 12 measuring positions are shown on top.

stopping power and the deposited energy per electron would be even lower.

2. Measurements at PSI

At PSI, the free-electron laser facility SwissFEL is currently under construction. An injector test facility is operated at a maximum energy of 300 MeV and serves as the principal test and demonstration plant for the SwissFEL project.[21]

The neutron H*(10) was measured at 12 positions inside the accelerator vault with a high photon background varying in intensity (Fig. 8).

The accelerator was operated at maximum electron energy of 230 MeV, with a repetition rate of 10 Hz. The electron beam, whose bunches were characterized by 200 pC charge and a few ps length, was stopped on a steel block shielded by concrete (beam dump). LUPIN-II was measuring in different conditions of the accelerator to test its capabilities in radiation fields with different photon contribution. For this purpose, the mode of operation of the electron gun and the radio-frequency cavities was varied. Figure 9 shows an acquisition performed close to the beam dump, where a significant pulsed photon component was accompanying the neutron field. The signal was acquired by setting a threshold on the current signal. The acquisition was triggered by the peak generated by the photon component of the stray field, whereas the neutrons generated in the dump were detected a few microseconds afterwards due to the TDT in the moderator. The photon peak corresponds, in terms of integrated charge, to several neutron interactions. One can profit from the different arrival times of the signals to implement an effective time-based discrimination technique. The photon peak can be used as a trigger for the acquisition, while the charge integration starts with a 5 μs delay, thus excluding the photon contribution. The reliability of this technique was statistically evaluated by verifying the results of the χ^2 test applied off-line to several acquisitions. As expected, the number of neutrons detected in each acquisition is a Poisson-distributed random variable, thus confirming that the residual charge obtained by neglecting the first 5 μs of the acquisition can be attributed to neutron interactions only. Further investigations are needed to better characterize this method, especially in the borderline situation where the photon peak is low and comparable to the neutron one (as expected near the electron gun). In this case it could be troublesome to identify whether the peak is generated by neutron or photon interactions.

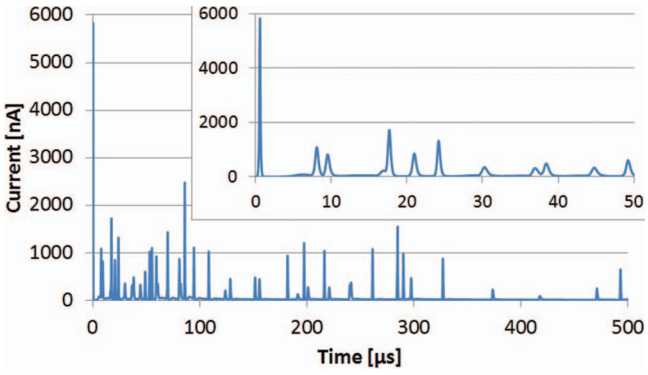

FIG. 9. Signal acquired at PSI in a neutron field characterized by an intense photon background (position "BD front"). The zoom of the first 50 μs shows the prompt photon peak.

IV. CONCLUSIONS

The modifications introduced in the new version of LUPIN-II allowed improving its performance both in terms of maximum detectable H*(10) per burst and of its discrimination properties. In particular, the results of the measurements showed that LUPIN-II:

- shows reduced space charge effects, due to the larger active volume of the BF_3 if compared to the ^{3}He employed in LUPIN; nevertheless, even if the sensitivity has been slightly reduced, it is still comparable with that of a conventional rem counter;
- has a non-isotropic geometrical response, which is limited to a $\pm$20% variation in the calibration factor;
- shows a slight H*(10) underestimation (<20%) for neutron bursts with an expected H*(10) up to 500 nSv; when employed in PNFs in operational conditions it shows the same performance of ionization chambers working in current mode;
- operates properly in high energy mixed fields, showing no significant deviation from the expected H*(10);
- can potentially discriminate the neutron/photon signal both in presence of a steady-state photon field and a mixed neutron/photon pulsed field.

LUPIN-II covers a lack in radiation protection instrumentation because up to now no active neutron detector possesses all the properties listed above. A future development of this detector will be oriented in finding solutions for coping with

the saturation effect. The detector is now working with a LabVIEW interface installed on a PC and the data analysis for neutron/photon discrimination is usually performed off-line. This issue will be solved by employing a Field Programmable Gate Array that can handle the on-line analysis in streaming and can manage two acquisition channels, one of which could be employed for the derivative technique.

ACKNOWLEDGMENTS

The authors wish to thank the HiRadMat team at CERN for their support during the measurements. This work has been supported by a Marie Curie Early Training Network Fellowship of the European Community's Seventh Framework Program under contract number PITN-GA-2011-289198-ARDENT.

[1]G. F. Knoll, *Radiation Detection and Measurement*, 4th ed. (John Wiley & Sons, Inc., 2010) , Chap. 4, p. 105.
[2]A. Klett and A. Leuschner, in *Proceedings of the IEEE 2006 Nuclear Science Symposium and Medical Imaging Conference*, San Diego, CA, 29 October–01 November (IEEE, San Diego, CA, 2007), Vol. 2, p. 806.
[3]A. L. Justus, Health Phys. **102**, 8 (2012).
[4]M. Ferrarini, V. Varoli, A. Favalli, M. Caresana, and B. Pedersen, Nucl. Instrum. Methods A **613**, 272 (2010).
[5]M. Caresana, M. Ferrarini, G. P. Manessi, M. Silari, and V. Varoli, Nucl. Instrum. Methods A **712**, 15 (2013).
[6]S. Rossi, Eur. Phys. J. Plus **126**, 78 (2011).
[7]I. Rios, J. Gonzalez, and R. E. Mayer, Radiat. Meas. **53–54**, 31 (2013).
[8]G. F. Knoll, *Radiation Detection and Measurement*, 4th ed. (John Wiley & Sons, Inc., 2010), Chap. 17, p. 649.
[9]M. Caresana, A. Denker, A. Esposito, M. Ferrarini, N. Golnik, E. Hohmann, A. Leuschner, M. Luszik-Bhadra, G. P. Manessi, S. Mayer, K. Ott, J. Rohrich, M. Silari, F. Trompier, M. Volnhals, and M. Wielunski, Nucl. Instrum. Methods A **737**, 203 (2014).
[10]E. Aza, M. Caresana, C. Cassell, N. Charitonidis, E. Harrouch, G. P. Manessi, M. Pangallo, D. Perrin, E. Samara, and M. Silari, Radiat. Meas. **61**, 25 (2014).
[11]C. Birattari, A. Ferrari, C. Nuccetelli, M. Pelliccioni, and M. Silari, Nucl. Instrum. Methods A **297**, 250 (1990).
[12]C. Birattari, A. Esposito, A. Ferrari, M. Pelliccioni, and M. Silari, Radiat. Prot. Dosim. **44**, 193 (1992).
[13]C. Birattari, A. Esposito, A. Ferrari, M. Pelliccioni, and M. Silari, Nucl. Instrum. Methods A **324**, 232 (1993).
[14]C. Birattari, A. Esposito, A. Ferrari, M. Pelliccioni, T. Rancati, and M. Silari, Radiat. Prot. Dosim. **76**, 135 (1998).
[15]E. Aza, M. Caresana, C. Cassell, V. Colombo, S. Damjanovic, S. Gilardoni, G. P. Manessi, M. Pangallo, D. Perrin, and M. Silari, Radiat. Prot. Dosim. (published online 2013).
[16]A. Fassò, A. Ferrari, J. Ranft, and P. R. Sala, CERN Technical Note, CERN-2005-10, INFN/TC_05/11, SLAC-R-773, 2005.
[17]G. Battistoni, S. Muraro, P. R. Sala, F. Cerutti, A. Ferrari, S. Roesler, A. Fassò, and J. Ranft, AIP Conf. Proc. **896**, 31 (2013).
[18]A. Mitaroff and M. Silari, Radiat. Prot. Dosim. **102**, 7 (2002).
[19]See supplementary material at http://dx.doi.org/10.1063/1.4879936 for full experimental and Monte Carlo results.
[20]M. Caresana, M. Helmecke, J. Kubancak, G. P. Manessi, K. Ott, R. Scherpelz, and M. Silari, Radiat. Prot. Dosim. (published online 2013).
[21]M. Pedrozzi, SwissFEL Injector Conceptual Design Report, PSI Report 10-05, 2010.